Published in final edited form as:

Nat Genet. 2013 September ; 45(9): 1050–1054. doi:10.1038/ng.2695.

Somatic and germline *CACNA1D* calcium channel mutations in aldosterone-producing adenomas and primary aldosteronism

Ute I. Scholl[1,2,15], **Gerald Goh**[1,2,15], **Gabriel Stölting**[3,15], **Regina Campos de Oliveira**[4], **Murim Choi**[1,2,5], **John D. Overton**[1,5], **Annabelle L. Fonseca**[6], **Reju Korah**[6], **Lee F. Starker**[6,7], **John W. Kunstman**[6], **Manju L. Prasad**[8], **Erum A. Hartung**[9], **Nelly Mauras**[10], **Matthew R. Benson**[10], **Tammy Brady**[11], **Jay R. Shapiro**[12], **Erin Loring**[1,2,5], **Carol Nelson-Williams**[1,2], **Steven K. Libutti**[13], **Shrikant Mane**[1,5], **Per Hellman**[7], **Gunnar Westin**[7], **Göran Åkerström**[7], **Peyman Björklund**[7], **Tobias Carling**[6,14], **Christoph Fahlke**[3], **Patricia Hidalgo**[3], and **Richard P. Lifton**[1,2,5]

[1]Department of Genetics, Yale University School of Medicine, New Haven, CT 06510, USA

[2]Howard Hughes Medical Institute, Yale University School of Medicine, New Haven, CT 06510, USA

[3]Institute of Complex Systems, Zelluläre Biophysik (ICS-4), Forschungszentrum Jülich, 52425 Jülich, Germany

[4]Institut für Neurophysiologie, Medizinische Hochschule Hannover, 30625 Hannover, Germany

[5]Yale Center for Mendelian Genomics, New Haven, CT 06510, USA

[6]Department of Surgery, Yale Endocrine Neoplasia Laboratory, Yale University School of Medicine, New Haven, CT 06510, USA

[7]Department of Surgical Sciences, Uppsala University, Uppsala, Sweden

[8]Department of Pathology, Yale University School of Medicine, New Haven, CT 06510, USA

[9]Children's Hospital of Philadelphia, Philadelphia, PA 19104, USA

[10]Nemours Children's Clinic, Jacksonville, Florida 32207, USA

[11]Johns Hopkins Pediatric Nephrology, Baltimore, MD 21287, USA

Correspondence to: Richard P. Lifton, M.D., Ph.D., Departments of Genetics and Internal Medicine, Howard Hughes Medical Institute, Yale University School of Medicine, 333 Cedar St., SHM I308, New Haven, CT 06510, USA. Telephone: +1-203-737-4420, Fax: +1-203-785-7560, richard.lifton@yale.edu.

[15]These authors contributed equally to this work.

Data access.

All somatic mutations found by exome sequencing are deposited in dbSNP under batch accession number 1059250.

Author contributions

ALF, LFS, JWK, MLP, EAH, NM, MRB, TB, JRS, EL, UIS, RPL, SKL, PHe, GW, GÅ, PB and TC ascertained and recruited patients, obtained samples and medical records; ALF, RK, LFS, UIS, PB and CNW prepared DNA and RNA samples and maintained sample archives; JDO and SM performed exome sequencing; UIS and GG performed and analyzed targeted DNA and RNA sequencing; GG, MC and RPL analyzed exome sequencing results; UIS and RK performed immunohistochemistry; UIS, GS, RCO, ChF and PHi made constructs and performed and analyzed electrophysiology; UIS, GG, GS, ChF, PHi and RPL wrote the manuscript.

Competing financial interests

The authors declare no competing financial interests.

[12]Osteogenesis Imperfecta Program, Kennedy Krieger Institute, Baltimore, MD 21205, USA

[13]Department of Surgery, Montefiore Medical Center and Albert Einstein College of Medicine, Bronx, NY 10467, USA

[14]Yale Cancer Center, Yale University School of Medicine, New Haven, CT 06510, USA

Abstract

Adrenal aldosterone-producing adenomas (APAs) constitutively produce the salt-retaining hormone aldosterone and are a common cause of severe hypertension. Recurrent mutations in the potassium channel *KCNJ5* that result in cell depolarization and Ca^{2+} influx cause ~40% of these tumors[1]. We found five somatic mutations (four altering glycine 403, one altering isoleucine 770) in *CACNA1D*, encoding a voltage-gated calcium channel, among 43 non-*KCNJ5*-mutant APAs. These mutations lie in S6 segments that line the channel pore. Both result in channel activation at less depolarized potentials, and glycine 403 mutations also impair channel inactivation. These effects are inferred to cause increased Ca^{2+} influx, the sufficient stimulus for aldosterone production and cell proliferation in adrenal glomerulosa[2]. Remarkably, we identified *de novo* mutations at the identical positions in two children with a previously undescribed syndrome featuring primary aldosteronism and neuromuscular abnormalities. These findings implicate gain of function Ca^{2+} channel mutations in aldosterone-producing adenomas and primary aldosteronism.

Aldosterone is normally produced in response to volume depletion (via angiotensin II signaling) or hyperkalemia[2]. Aldosterone signaling defends intravascular volume by increasing intestinal and renal Na-Cl absorption and reabsorption, respectively. Constitutive production of aldosterone (primary aldosteronism) results in hypertension, often associated with hypokalemia[3]. About 5% of patients referred to hypertension clinics (1 to 10 million people world-wide) have aldosterone-producing adenomas (APAs)[3,4]. APAs are typically benign, well-circumscribed and solitary; their removal cures or ameliorates hypertension. *KCNJ5* mutations alter channel selectivity, allowing Na^+ conductance. This results in cell depolarization, activation of voltage-gated Ca^{2+} channels, aldosterone production and cell proliferation. These mutations are inferred to be sufficient for APA formation because rare patients with Mendelian aldosteronism and massive adrenal hyperplasia have identical *KCNJ5* mutations in their germline[1,5].

We performed exome sequencing of 14 APAs and matched germline DNA. All patients had hypertension with elevated aldosterone levels despite suppressed plasma renin activity (PRA) and a pathologic diagnosis of APA (Supplementary Table 1). Four previously sequenced APAs[1] were added to subsequent analysis (total 18 APAs). Samples were sequenced to high coverage and somatic mutations were called (**Online Methods**, Supplementary Table 2). The mean somatic mutation rate was 3.0×10^{-7} per base, with a mean of 1.7 silent and 6.1 protein-altering somatic mutations per tumor (median 1 and 3.5, respectively; Supplementary Fig. 1). Five of these 18 APAs had disease-causing mutations in *KCNJ5* (p.Gly151Arg or p.Leu168Arg), and one had a known gain of function mutation, *CTNNB1* (p.Ser45Phe), previously found in adrenocortical tumors[6].

One gene, *CACNA1D*, had somatic mutations in more than one APA (missense mutations p.Gly403Arg (NM_001128840.2:c.1207G>C) and p.Ile770Met (NM_000720.3:c.2310C>G; and in different isoform NM_001128840.2:c.2250C>G)), both in tumors without *KCNJ5* or *CTNNB1* mutations) (Fig. 1). Both mutations are previously undescribed (absent among >10,000 exomes in public and Yale databases), apparently heterozygous, and confirmed by direct Sanger sequencing (Fig. 1a). Both occurred in tumors with few protein-altering somatic mutations (4 and 2, respectively) (Supplementary Table 3) and zero detected copy number variants (CNVs). *CACNA1D* encodes $Ca_V1.3$, the α_1 (pore-forming) subunit of an L-type (long-lasting) voltage-gated calcium channel. These α_1 subunits contain 4 repeated domains (I-IV) (Fig. 2), each with 6 transmembrane segments (S1-S6) and a membrane-associated loop between S5 and S6. S5, S6 and the interposed loop line the channel pore[7]. The two *CACNA1D* mutations occur in similar positions near the cytoplasmic ends of S6 segments of domains I and II (Fig. 1c, Fig. 2).

Direct Sanger sequencing of all the S6 segments in *CACNA1D* in 46 additional APAs, including highly similar alternative splice isoforms of the first S6 segment (encoded by alternative exons 8A and 8B[8]) identified three additional somatic mutations in these segments. Most interestingly, two were the same Gly403Arg mutation in exon 8A found by exome sequencing, and one produced the homologous Gly403Arg mutation in exon 8B. Further sequencing identified 16 additional tumors with Gly151Arg or Leu168Arg mutations in *KCNJ5* and one additional *CTNN1B* mutation (p.Ser45Pro). All *CACNA1D* mutations occurred in tumors without *KCNJ5* or *CTNN1B* mutations. Collectively, *CACNA1D* mutations were identified in 5 of 64 APAs (7.8%), including 5/41 without *KCNJ5* or *CTNNB1* mutations (12.2%). The probability of finding the identical somatic mutation at any base in the exome 3 times by chance among 64 tumors, given the observed somatic mutation rate, is 3.0×10^{-8}; including the tumor with somatic mutation at the homologous base in exon 8B, the probability of seeing either of these mutations in 4 of 64 tumors is 2.2×10^{-12} (**Online Methods**).

Gly403 and Ile770 are completely conserved in orthologs from invertebrates to humans (Fig. 1c). Additionally, Ile770 is conserved in all paralogs (Fig. 1c). Interestingly, Gly403 is conserved among all paralogs that are activated by large depolarizing potentials (high-voltage-activated), but not among channels activated by small changes in membrane potential (low-voltage-activated) (Fig. 1c). The finding of recurrent and clustered somatic *CACNA1D* mutations strongly suggests a gain of function mechanism.

While *CACNA1H* ($Ca_V3.2$) has been implicated in cyclic glomerulosa cell membrane potential oscillations and aldosterone secretion[9], little is known about the role of *CACNA1D* ($Ca_V1.3$). Wild-type and mutant *CACNA1D* alleles are expressed in tumor cDNA (Fig. 1a). Moreover, analysis of normal human adrenocortical RNA[1] revealed that *CACNA1D* was the most highly expressed Ca^{2+} channel subunit, followed by β_2 (*CACNB2*) and $\alpha_2\delta_1$ (*CACNA2D1*) subunits (Supplementary Table 4). Additionally, immunohistochemistry with 3 anti-CACNA1D ($Ca_V1.3$) antibodies demonstrated expression in human zona glomerulosa (Fig. 3, Supplementary Fig. 2). These findings support a role for $Ca_V1.3$ in normal adrenal cortex and APA.

To assess the effect of *CACNA1D* mutations on channel function, we expressed wildtype (WT) and mutant $Ca_V1.3$ together with β_2 (β_{2a} isoform) and $\alpha_2\delta_1$ subunits in HEK293T cells. Figure 4a shows representative whole-cell patch clamp recordings. Upon depolarizing voltage steps, $Ca_V1.3^{WT}$ calcium currents showed fast activation, followed by a slow decay caused by voltage-dependent (VDI) and calcium-dependent inactivation (CDI)[10] (Supplementary Fig. 3). Compared to WT channels, the Gly403Arg mutant ($Ca_V1.3^{G403R}$) and Ile770Met mutant ($Ca_V1.3^{I770M}$) both showed maximum current amplitudes at less depolarized potentials (Fig. 4b). $Ca_V1.3^{WT}$ exhibited a half-maximal activation voltage ($V_{½}$) at −9.2 ± 1.0 mV (s.e.m., $n = 7$), while $V_{½}$ for $Ca_V1.3^{G403R}$ and $Ca_V1.3^{I770M}$ was −25.6 ± 2.5 mV ($n = 7$, $P < 0.001$ versus WT) and −31.7 ± 1.1 mV ($n = 6$, $P < 0.001$ versus WT) respectively, indicating that these mutations facilitated channel opening (Fig. 4b). Current densities are shown in Supplementary Figure 4.

The Gly403Arg mutation also drastically impaired inactivation of $Cav1.3^{WT}$ (Fig. 4a), suggesting a role for sustained activation with this mutation. $Ca_V1.3^{I770M}$ showed inactivation shifted to more hyperpolarized potentials (Fig. 4a, 4c, Supplementary Fig. 3).

By analogy to *KCNJ5*, we considered possible germline *CACNA1D* mutations. We sequenced *CACNA1D* S6 segments of domains I and II in 100 unrelated subjects with unexplained early-onset primary aldosteronism. Remarkably, we found mutations altering the same amino acids mutated in APAs in 2 subjects – one (1441-1) with a Gly403Asp mutation in exon 8B, and another (1555-1) with the Ile770Met mutation (Fig. 1b). Neither has been seen previously in SNP or exome databases. Both were *de novo* mutations as they were absent in their parents, with genotyping of nine highly polymorphic short tandem repeat markers providing unequivocal evidence of maternity/paternity (Supplementary Table 5). The probability of finding by chance two *de novo* mutations in any of the 3 *CACNA1D* codons mutated in APAs among 100 test cases is 3.8×10^{-11} (**Online Methods**), implicating these *de novo* mutations in disease pathogenesis. Electrophysiology of the germline p.Gly403Asp mutation ($Ca_V1.3^{G403D}$) in subject 1444-1 demonstrated activation at less depolarizing potentials ($V_{1/2} = -32.4 \pm 2.3$ mV ($n = 5$, $P < 0.001$ versus WT)) and markedly impaired inactivation – similar to Gly403Arg (Fig. 4).

Subject 1444-1 was diagnosed with hypertension at birth (blood pressure 119/78 mmHg; >99th percentile) with biventricular hypertrophy, a ventricular septal defect, pulmonary hypertension, and second-degree heart block. Aldosterone was elevated (128.6 ng/dL) with low plasma renin activity (PRA, 0.78 ng/ml/h) and high aldosterone:renin ratio (ARR, 165, >30 consistent with primary aldosteronism). The clinical course was notable for uncontrolled hypertension with hypokalemia (serum K^+ 3.3 mmol/L, normal 3.5–5.6). Interestingly, treatment with a calcium channel blocker, amlodipine, normalized blood pressure, and biventricular hypertrophy resolved. Other features included a seizure disorder, apparent cerebral palsy, cortical blindness, and complex neuromuscular abnormalities. There was no significant family history (Supplementary Note).

Subject 1555-1 was diagnosed at birth with cerebral palsy, spastic quadriplegia, mild athetosis, severe generalized intellectual disability, and complex partial and generalized seizures. At age 5 years, she was markedly hypertensive (132/90 mmHg; >99th percentile),

with retrospective recognition of persistently elevated blood pressure and polydipsia. She had hypokalemia (serum K^+ 2.8 mmol/L) and metabolic alkalosis (bicarbonate 30 mmol/L). Serum aldosterone was high (36 ng/dL), despite suppressed PRA (0.15 ng/mL/h; ARR 240). CT scan showed no adrenal abnormality, and echocardiogram showed mild left ventricular hypertrophy. She was treated with clonidine, and later spironolactone. There was no significant family history (Supplementary Note).

These results implicate recurrent gain of function mutations in *CACNA1D* in ~8% of APAs and a new Mendelian syndrome featuring primary aldosteronism associated with seizures and neuromuscular disease. The finding of *de novo* germline mutations at the same positions as somatic mutations found in APAs is consistent with these single mutations being sufficient for production of APA, analogous to findings with *KCNJ5*[1]. These findings indicate that APAs are commonly caused by single mutations and have implications for other hormone-producing tumors. Moreover, they underscore the discovery of novel biology in a range of benign tumors[1,11].

Electrophysiological studies of mutant $Ca_V1.3$ channels implicate increased Ca^{2+} influx in disease pathogenesis (Supplementary Fig. 5). Mutant channels activate at membrane potentials closer to the glomerulosa resting potential (about −82 mV[9]); moreover, inactivation of $Ca_V1.3^{G403R}$ and $Ca_V1.3^{G403D}$ is impaired. Spontaneous glomerulosa membrane potential oscillations[9] may contribute to activation of these mutant channels. While increased current densities were seen with $Ca_V1.3^{I770M}$ and $Ca_V1.3^{G403D}$, this was not the case for $Ca_V1.3^{G403R}$ (Supplementary Fig. 4). Because high Ca^{2+} influx may increase cell lethality, one must interpret differences in current density with caution. Further studies of the properties of single channels and the impact of these mutations in engineered animal models will be of interest.

Increased Ca^{2+} influx due to *CACNA1D* mutations phenocopies the consequence of *KCNJ5* mutations, which cause increased Ca^{2+} influx by depolarizing glomerulosa cells. This suggests increased intracellular Ca^{2+} as a final common pathway to APA formation. These findings have implications for other hormone-secreting tumors and endocrinopathies in which hormone secretion is regulated by Ca^{2+}.

While the mutations described herein are gain of function, homozygous loss of function mutations in *CACNA1D* in mice and humans result in deafness, bradycardia and arrhythmia[8,12].

Interestingly, mutations in S6 segments of other L-type Ca^{2+} channels cause disease by similar gain of function effects[13]. Germline mutations altering the positions homologous to Gly403 and Ile770 in *CACNA1F* cause congenital stationary night blindness type 2[14,15]; similarly, mutation at the position homologous to Gly403 in *CACNA1C* causes Timothy syndrome[16] (Fig. 1c). Finally, gain of function mutations in S6 segments of *CACNA1A* cause familial hemiplegic migraine[17,18].

While only a small number of APAs with *CACNA1D* mutations have been identified, tumors with *CACNA1D* mutations were significantly smaller than those with *KCNJ5* mutations (13.4 ± 4.8 mm versus 21.9 ± 7.4 mm, s.d., $P = 0.01$), and there was a trend toward older

age at presentation (53.8 ± 9.0 versus 43.6 ± 10.7 years, $P = 0.06$). Unlike *KCNJ5* mutations[1,19], *CACNA1D* mutations did not show a strong female bias (3/30 males, 2/34 females).

The subjects with *de novo* activating *CACNA1D* mutations represent a previously undescribed Mendelian syndrome featuring primary aldosteronism. While additional cases will be required to fully define the extraadrenal manifestations of this syndrome, their complicated neuromuscular histories indicate a multisystem disease, consistent with *CACNA1D* expression in neurons and heart[8]. The absence of adrenal hyperplasia by CT scan in subject 1555-1 at age 9 is noteworthy. Different germline mutations at the identical position in *KCNJ5* are associated with aldosteronism with or without adrenal hyperplasia owing to variable Na^+ conductance resulting in varying cell lethality – patients with mutations causing high cell lethality never develop adrenal hyperplasia[5]. Further work will be required to establish whether the absence of hyperplasia with germline *CACNA1D* mutation relates to high cell lethality.

Following submission of this paper, recurrent mutations in *ATP1A1* (the α subunit of the Na^+/K^+ ATPase) and *ATP2B3* (a plasma membrane Ca^{2+} ATPase) that account for 5.2% and 1.6% of APAs, respectively, were reported[20]. We sequenced these positions in our cohort and found described mutations in 3 subjects (4.7%, Supplementary Table 1).

Lastly, the apparent response to treatment with a calcium channel blocker in subject 1444-1 raises the possibility of specific treatment for patients with APAs and *CACNA1D* mutations. Approved calcium channel blockers are weak antagonists of wildtype $Ca_V1.3$ although potent and specific $Ca_V1.3$ inhibitors have been identified[21]. Such compounds, or others that are selective for recurrent mutations, may have particular promise in the treatment of a subset of patients with *CACNA1D* mutations.

Online Methods

Subjects

Matched APA and venous blood DNAs were obtained from patients undergoing adrenalectomy for hypertension with primary aldosteronism and adrenocortical tumor at Yale New Haven Hospital, Uppsala University Hospital, and Montefiore Medical Center and Albert Einstein College of Medicine, and were evaluated as previously described[1]. Additional APAs and matched normal samples were obtained from paraffin-embedded samples in Yale Department of Pathology. Additionally, patients with unexplained early onset aldosteronism, including parents in selected cases, were also studied. The research protocols were approved by local IRBs and informed consent was obtained from all research participants.

DNA preparation, genotyping and exome sequencing

Genomic DNA was prepared from venous blood, tumor and surrounding normal tissue by standard procedures. For FFPE samples, DNA was prepared using the QiaAmp DNA FFPE tissue kit (Qiagen) according to the manufacturer's instructions.

Targeted capture of exome sequences was performed using the 2.1M NimbleGen Exome reagent followed by sequencing on the Illumina platform as previously described[1]. Somatic mutations were called based on the significance of differences in read distributions between matched tumor and blood samples[1]. Calls were further evaluated by manual inspection of the read alignments. The somatic mutation rate was calculated from the observed number of somatic mutations and the number of coding bases in the exome capture.

Tumor purity was calculated from the mean minor allele frequency (MAF) of all high quality SNPs in regions of LOH. For tumors with no detectable region of LOH, purity was estimated from mean MAF of inferred heterozygous somatic variants.

Copy number variants were called from the normalized ratio of coverage depth comparing tumor and normal samples, and changes in MAF at informative SNPs.

Statistical tests

Two-tailed t-tests were used for statistical analysis of tumor characteristics. P-values for the occurrence of observed mutations by chance were calculated as binomial probabilities from the number of occurrences of specific mutations, the number of tumors studied, the observed somatic mutation rate, and the total number of exonic bases. For statistical analysis of the voltage dependence of activation in WT and mutant channels, $V_{1/2}$ values were tested for equality of variances and normality (Shapiro-Wilk method) and compared using pairwise multiple comparison procedures (Holm-Sidak method).

Sanger sequencing of genomic DNA

Direct bidirectional Sanger sequencing of *CACNA1D* from genomic DNA in tumor-blood pairs was performed following PCR amplification using specific primers. All S6 segments of *CACNA1D* were sequenced in all APAs; the S6 segments of domains I and II were sequenced for germline mutations in patients with early-onset hypertension. Positions with recurrent mutations in *KCNJ5, CTNNB1*, *ATP1A1* and *ATP2B3* were sequenced in APAs following amplification by PCR using specific primers. Primer sequences are listed in Supplementary Table 6.

Genotyping of parent-offspring trios

Nine highly polymorphic markers (loci CSF1PO, D135317, D16S539, D18S51, D7S820, D8S1179, TH01, TPOX, and D195433) were genotyped in parent-offspring trios of kindreds 1444 and 1555 by PCR amplification using specific primers followed by direct Sanger sequencing. Genotypes were scored by the number of repeats present on each allele as independently assessed by two investigators; genotype calls were concordant for all markers. Paternity and maternity indices were separately calculated for each putative parent[23] using allele frequencies determined in 258 African Americans or 302 individuals of European descent[24].

TOPO cloning of PCR products

DNA was amplified using the G403R_F and G403R_R primers, and PCR products were cloned using the TOPO TA Cloning Kit (Invitrogen). Plasmid DNA from individual colonies was amplified by PCR and Sanger sequenced using the G403R_F primer.

cDNA synthesis and sequencing

Total RNA was prepared from fresh-frozen tissue using the AllPrep DNA/RNA/Protein Mini Kit (Qiagen) or the TRIzol Reagent (Invitrogen), followed by column purification and DNase digestion using the RNeasy Mini Kit (Qiagen). Reverse transcription of 100 ng RNA was performed with Oligo(dT)$_{12\text{-}18}$ priming (Invitrogen) using Superscript III Reverse Transcriptase (Invitrogen). cDNA was amplified using intron-spanning primers G403RTF/R and I770RTF/R and sequenced with forward and reverse primers.

Immunohistochemistry

5 μM sections from formalin-fixed paraffin-embedded normal human adrenal cortex (2 patients) were obtained from the Yale Pathology Tissue Service. Sections were deparaffinized and epitope retrieval was performed by heating in 10 mM sodium citrate in a microwave. Endogenous peroxidase activity was quenched with 0.3–3% H_2O_2, and samples were permeabilized in 1% SDS in TBS or 0.2% Triton X-100 in PBS. After blocking, slides were incubated with anti-CACNA1D (#HPA020215, Sigma; 1:100 dilution), anti-Dab2 (#sc-13982, Santa Cruz; 1:100 dilution), anti-L-type Ca^{++} CP α1D (#sc-32071, Santa Cruz, 1:50–1:100 dilution) or anti-$Ca_V1.3$ (#ACC-005, Alomone, 1:100–1:250 dilution) for 12 hours. Horseradish peroxidase-conjugated anti-rabbit or anti-goat secondary antibody and DAB were used to visualize the signal. Where signal was low, a biotinylated secondary antibody was used, followed by HRP streptavidin. For Alomone and Santa Cruz antibodies, immunizing peptides were tested for their ability to block antibody labeling of tissues following manufacturer's protocols; incubations with and without immunizing peptides were processed in parallel. Sections were counterstained with haematoxylin. Images were captured using a Zeiss Axio Imager M2 microscope and processed using AxioVision software (Rel. 4.8) and Adobe Photoshop.

Molecular Cloning

The canonical isoform of human *CACNA1D* in pCMV6-XL6 was obtained from Origene (#SC309716, NM_000720.1). This isoform contains exon 8B. Other isoforms (NM_001128840.2 and NM_001128839.2) have all the same domain structures but vary in the presence of exons 11, 32 and 44 in extracellular and intracellular segments.

Site-directed mutagenesis (Quikchange, Stratagene) was performed to introduce the Gly403Arg, Ile770Met and Gly403Asp mutations into *CACNA1D*. Each construct was validated by sequencing of the complete coding region. The $Ca_V\beta_{2a}$ coding region (Swiss-Prot accession number Q8VGC3-2) was fused at its carboxy-terminal end to mCherry and subcloned into the pcDNA3.1 vector. The $Ca_V\alpha_2\delta_1$ cDNA in the pIRES-dsRed vector was kindly provided by Dr. Frank Lehmann-Horn (University of Ulm, Germany).

Plasmids were prepared using the HiSpeed Plasmid Maxi Kit (Qiagen).

Transient transfection and electrophysiological recordings

HEK293T cells (The European Collection of Cell Cultures) were grown to 80% confluence on 10 cm dishes in Dulbecco's modified Eagle's medium supplemented with 10% fetal bovine serum, L-glutamine (2 mM), penicillin G (100 units/ml), and streptomycin (10 mg/ml) and incubated in a 5% CO_2 humidified atmosphere. Cells were co-transfected with 1 μg of β_{2a}-mCherry, 1 μg of $\alpha_2\delta_1$ and 2 μg of *CACNA1D* WT, Gly403Asp, Gly403Arg, or Ile770Met expression plasmids using Lipofectamine LTX (Life Technologies). Currents were recorded from transfections with plasmids from at least two preparations of each *CACNA1D* construct. Cells were split 24 h after transfection. Currents were recorded on a HEKA EPC 10 amplifier (HEKA Elektronik) using the Patchmaster software. Borosilicate pipettes with resistances of 1–3 MΩ were pulled on a Sutter P-97 puller (Harvard Apparatus) and fire-polished using a Narishige MF-900 microforge. The extracellular solution contained: 5 mM $CaCl_2$, 125 mM TEA-Cl, 10 mM HEPES, 15 mM Mannitol, pH 7.4. Pipette solution contained: 100 mM CsCl, 5 mM TEA-Cl, 3.6 mM PCr-Na_2, 10 mM EGTA, 5 mM Mg-ATP, 0.2 mM Na-GTP, 10 mM HEPES, pH 7.4 (titration with CsOH). Currents were elicited by 1–2 s voltage pulses ranging from −70 mV to +20 mV in 10 mV increments from a holding potential of −80 mV[25]. No visible calcium currents were recorded in cells transfected with β_{2a} and $\alpha_2\delta_1$ subunits alone. Only recordings with distinct currents in the presence of external Ca^{2+} or Ba^{2+} that stayed stable over the recording duration were used for analysis.

Data were filtered at 3 kHz. Peak current amplitudes depend on the voltage dependences of the open probability and the unitary current. Since calcium channels exhibit a constant unitary conductance under our experimental conditions, the voltage dependences of activation were obtained by fitting a plot of the current-voltage relation according to:

$$I(V)=G\cdot(V-V_{rev})\cdot\frac{1}{1+e^{\frac{-(V-V_{1/2})}{k}}} \quad (1)$$

with I being the macroscopic current, G the maximum conductance, V the voltage, V_{rev} the reversal potential, $V_{1/2}$ the half-maximal activation and k the slope. Plots of the relative open probabilities of activation were calculated by dividing peak-current voltage plots by the normalized maximum conductance ($I_{peak}/(V-V_{rev})$)[26] and fitted with the Boltzmann function according to:

$$P_{open}(V)=\frac{1}{1+e^{\frac{-(V-V_{1/2})}{k}}} \quad (2)$$

with P_{open} being the open probability at the desired voltage.

The time course of inactivation[10] was determined by fitting the current decay after activation with a bi-exponential function:

$$I(t)=A_0+A_1\cdot e^{-\frac{t}{\tau_1}}+A_2\cdot e^{-\frac{t}{\tau_2}} \quad (3)$$

with A being the amplitude of the individual components, t the time and τ the corresponding time constants. The residual amplitude A_0 corresponds to the steady state current at the given potential. The voltage dependence of the ratio of A_0 by I_{peak} provides the steady-state inactivation curve that was fitted with a Boltzmann function[27].

Data were analyzed in FitMaster (HEKA Elektronik) and SigmaPlot (Jandel Scientific).

Orthologs and paralogs

Orthologs or close paralogs of CACNA1D in vertebrate and invertebrate species were identified by a BLAST search[1]. GenBank accession numbers were: NP_001122311.1 (human isoform c), NP_000711.1 (human isoform a), NP_001077085.1 (mouse), NP_990365.1 (chicken), XP_002938148.1 (frog), NP_982351.1 (zebrafish), and XP_002123864.1 (tunicate). For human α_1 subunit paralogs, GenBank accession numbers were: NP_000060.2 (CACNA1S), NP_955630.2 (CACNA1C), NP_005174.2 (CACNA1F), NP_000059.3 (CACNA1A), NP_000709.1 (CACNA1B), NP_001192222.1 (CACNA1E), NP_061496.2 (CACNA1G), NP_066921.2 (CACNA1H), and NP_066919.2 (CACNA1I).

Adrenal Cortical Gene Expression

Calcium channel expression in human adrenal cortex was extracted from a previously described dataset[1].

Supplementary Material

Refer to Web version on PubMed Central for supplementary material.

Acknowledgments

We thank the patients and families whose participation made this study possible. We thank the staff of the Yale West Campus Genomics Center, the Yale Cellular and Molecular Physiology Microscopy and Imaging Core, the Endocrine Surgical Laboratory, Clinical Research Centre, Uppsala University Hospital and the Department of Surgery, Montefiore Medical Center and Albert Einstein College of Medicine, for their invaluable contributions to this research. Drs. Jan Matthes (Universität Köln, Germany) and Frank Lehmann-Horn (Universität Ulm, Germany) kindly provided us with $\alpha_2\delta$ subunit clones. Supported by the NIH Centers for Mendelian Genomics (5U54HG006504), the Fondation Leducq Transatlantic Network in Hypertension, the Deutsche Forschungsgemeinschaft and by the Swedish Cancer Society, the Swedish Research Council, and the Lions Cancer Fund, Uppsala. GG is supported by the Agency for Science, Technology and Research, Singapore. TC is a Doris Duke-Damon Runyon Clinical Investigator. RPL is an Investigator of the Howard Hughes Medical Institute.

References

1. Choi M, et al. K+ channel mutations in adrenal aldosterone-producing adenomas and hereditary hypertension. Science. 2011; 331:768–72. [PubMed: 21311022]
2. Spat A, Hunyady L. Control of aldosterone secretion: a model for convergence in cellular signaling pathways. Physiol Rev. 2004; 84:489–539. [PubMed: 15044681]
3. Rossi GP, et al. A prospective study of the prevalence of primary aldosteronism in 1,125 hypertensive patients. J Am Coll Cardiol. 2006; 48:2293–300. [PubMed: 17161262]
4. Conn JW. Presidential address. I Painting background II Primary aldosteronism, a new clinical syndrome. J Lab Clin Med. 1955; 45:3–17. [PubMed: 13233623]
5. Scholl UI, et al. Hypertension with or without adrenal hyperplasia due to different inherited mutations in the potassium channel KCNJ5. Proc Natl Acad Sci U S A. 2012; 109:2533–8. [PubMed: 22308486]

6. Tadjine M, Lampron A, Ouadi L, Bourdeau I. Frequent mutations of beta-catenin gene in sporadic secreting adrenocortical adenomas. Clin Endocrinol (Oxf). 2008; 68:264–70. [PubMed: 17854394]
7. Catterall WA. Signaling complexes of voltage-gated sodium and calcium channels. Neurosci Lett. 2010; 486:107–16. [PubMed: 20816922]
8. Baig SM, et al. Loss of Ca(v)1.3 (CACNA1D) function in a human channelopathy with bradycardia and congenital deafness. Nat Neurosci. 2011; 14:77–84. [PubMed: 21131953]
9. Hu C, Rusin CG, Tan Z, Guagliardo NA, Barrett PQ. Zona glomerulosa cells of the mouse adrenal cortex are intrinsic electrical oscillators. J Clin Invest. 2012; 122:2046–53. [PubMed: 22546854]
10. Tadross MR, Ben Johny M, Yue DT. Molecular endpoints of Ca2+/calmodulin- and voltage-dependent inactivation of Ca(v)1.3 channels. J Gen Physiol. 2010; 135:197–215. [PubMed: 20142517]
11. Clark VE, et al. Genomic analysis of non-NF2 meningiomas reveals mutations in TRAF7, KLF4, AKT1, and SMO. Science. 2013; 339:1077–80. [PubMed: 23348505]
12. Platzer J, et al. Congenital deafness and sinoatrial node dysfunction in mice lacking class D L-type Ca2+ channels. Cell. 2000; 102:89–97. [PubMed: 10929716]
13. Hering S, et al. Pore stability and gating in voltage-activated calcium channels. Channels (Austin). 2008; 2:61–9. [PubMed: 18849656]
14. Hoda JC, Zaghetto F, Koschak A, Striessnig J. Congenital stationary night blindness type 2 mutations S229P, G369D, L1068P, and W1440X alter channel gating or functional expression of Ca(v)1.4 L-type Ca2+ channels. J Neurosci. 2005; 25:252–9. [PubMed: 15634789]
15. Hemara-Wahanui A, et al. A CACNA1F mutation identified in an X-linked retinal disorder shifts the voltage dependence of Cav1.4 channel activation. Proc Natl Acad Sci U S A. 2005; 102:7553–8. [PubMed: 15897456]
16. Splawski I, et al. Severe arrhythmia disorder caused by cardiac L-type calcium channel mutations. Proc Natl Acad Sci U S A. 2005; 102:8089–96. discussion 8086–8. [PubMed: 15863612]
17. Hans M, et al. Functional consequences of mutations in the human alpha1A calcium channel subunit linked to familial hemiplegic migraine. J Neurosci. 1999; 19:1610–9. [PubMed: 10024348]
18. Battistini S, et al. A new CACNA1A gene mutation in acetazolamide-responsive familial hemiplegic migraine and ataxia. Neurology. 1999; 53:38–43. [PubMed: 10408534]
19. Scholl UI, Lifton RP. New insights into aldosterone-producing adenomas and hereditary aldosteronism: mutations in the K+ channel KCNJ5. Curr Opin Nephrol Hypertens. 2013; 22:141–7. [PubMed: 23318698]
20. Beuschlein F, et al. Somatic mutations in ATP1A1 and ATP2B3 lead to aldosterone-producing adenomas and secondary hypertension. Nat Genet. 2013; 45:440–4. [PubMed: 23416519]
21. Kang S, et al. Ca(V)1.3-selective L-type calcium channel antagonists as potential new therapeutics for Parkinson's disease. Nat Commun. 2012; 3:1146. [PubMed: 23093183]
22. Peloquin JB, Rehak R, Doering CJ, McRory JE. Functional analysis of congenital stationary night blindness type-2 CACNA1F mutations F742C, G1007R, and R1049W. Neuroscience. 2007; 150:335–45. [PubMed: 17949918]
23. Brenner CH. A note on paternity computation in cases lacking a mother. Transfusion (Paris). 1993; 33:51–4.
24. Butler JM, Schoske R, Vallone PM, Redman JW, Kline MC. Allele frequencies for 15 autosomal STR loci on U.S. Caucasian, African American, and Hispanic populations. J Forensic Sci. 2003; 48:908–11. [PubMed: 12877323]
25. Gonzalez-Gutierrez G, et al. The guanylate kinase domain of the beta-subunit of voltage-gated calcium channels suffices to modulate gating. Proc Natl Acad Sci U S A. 2008; 105:14198–203. [PubMed: 18776052]
26. Marcantoni A, et al. Loss of Cav1.3 channels reveals the critical role of L-type and BK channel coupling in pacemaking mouse adrenal chromaffin cells. J Neurosci. 2010; 30:491–504. [PubMed: 20071512]
27. Roberts-Crowley ML, Rittenhouse AR. Arachidonic acid inhibition of L-type calcium (CaV1.3b) channels varies with accessory CaVbeta subunits. J Gen Physiol. 2009; 133:387–403. [PubMed: 19332620]

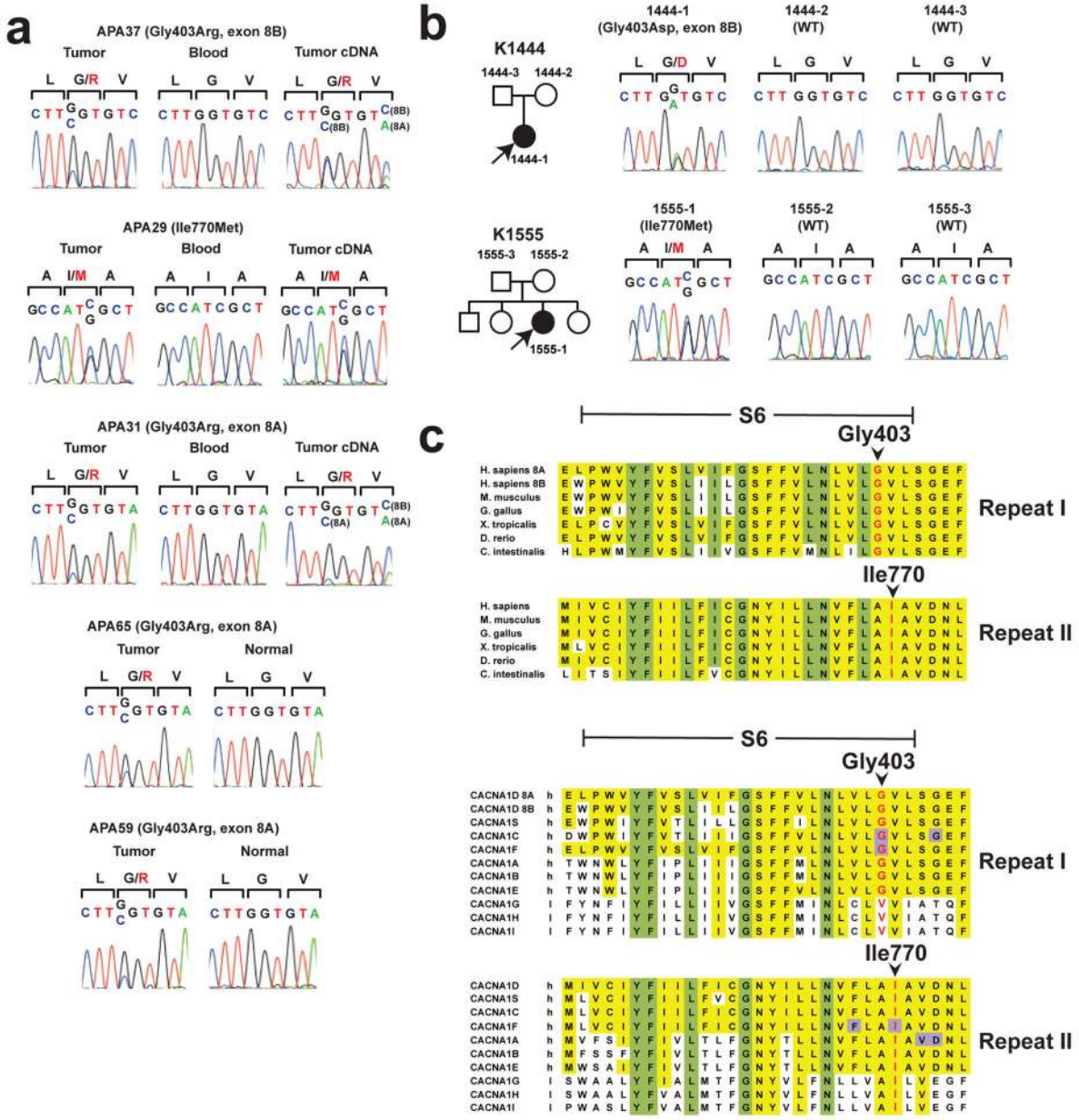

Figure 1.

CACNA1D mutations in aldosterone-producing adenomas and primary aldosteronism. (**a**) Sequences of tumor and blood genomic DNA, and (where available) tumor cDNA, of *CACNA1D* codons 402–404 in APA37, APA31, APA65 and APA59, and of codons 769–771 in APA29. Mutations are present in tumor only, and expressed in cDNA. Sequencing the products of cloned PCR products confirmed the presence of identified mutations in APAs 31, 65 and 59. (**b**) Pedigrees of kindreds with germline *CACNA1D* mutations. Affected individuals are shown as filled symbols. The corresponding Sanger sequences are depicted to the right. (**c**) Conservation of Gly403 and Ile770 in orthologs and paralogs. S6, S6 segment; 'h', high-voltage activated; 'l', low-voltage activated. Residues conserved

among all homologs are marked in yellow, and positions conserved in ≥90% of all homologs in both repeats are marked in green. Residues associated with known gain of function mutations in human diseases[14–17,22] are marked in purple.

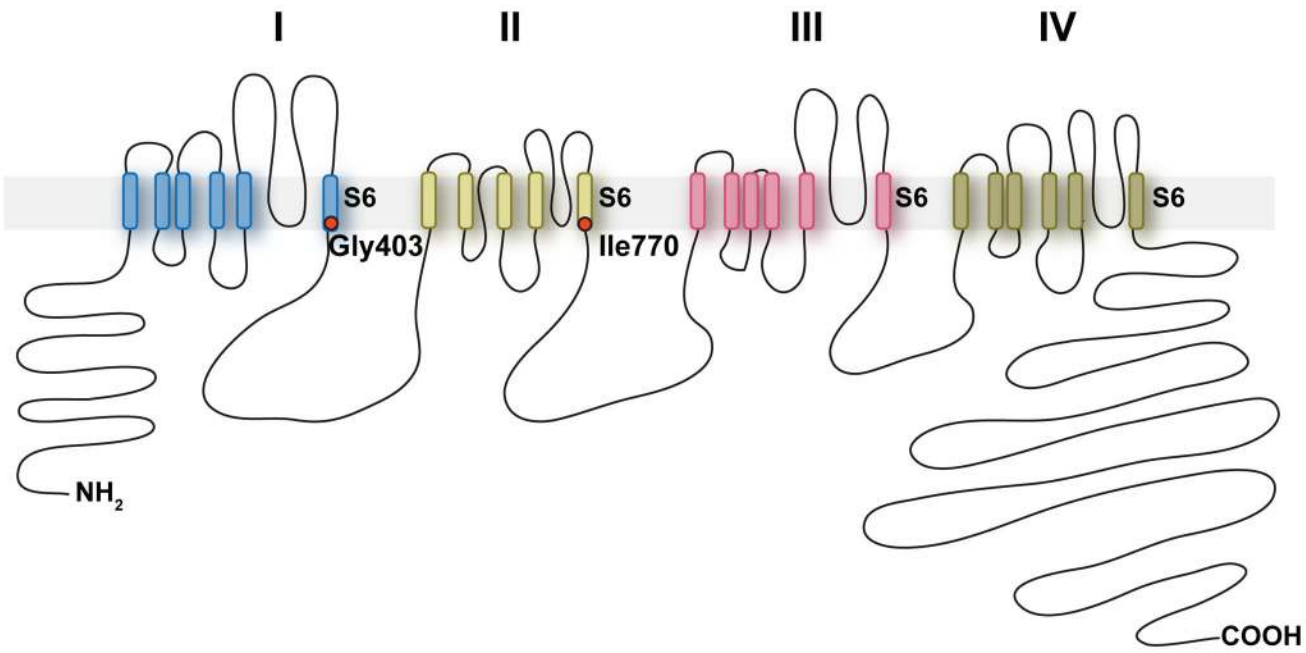

Figure 2.

Transmembrane structure of $Ca_V1.3$. *CACNA1D* encodes the pore-forming α_1 subunit of a voltage-gated calcium channel. These channels feature four homologous repeats (I–IV) with 6 transmembrane segments (S1-S6) and a membrane-associated loop between segments S5 and S6. The five APA and two germline *CACNA1D* mutations identified in this study are located at the end of S6 segments implicated in channel gating.

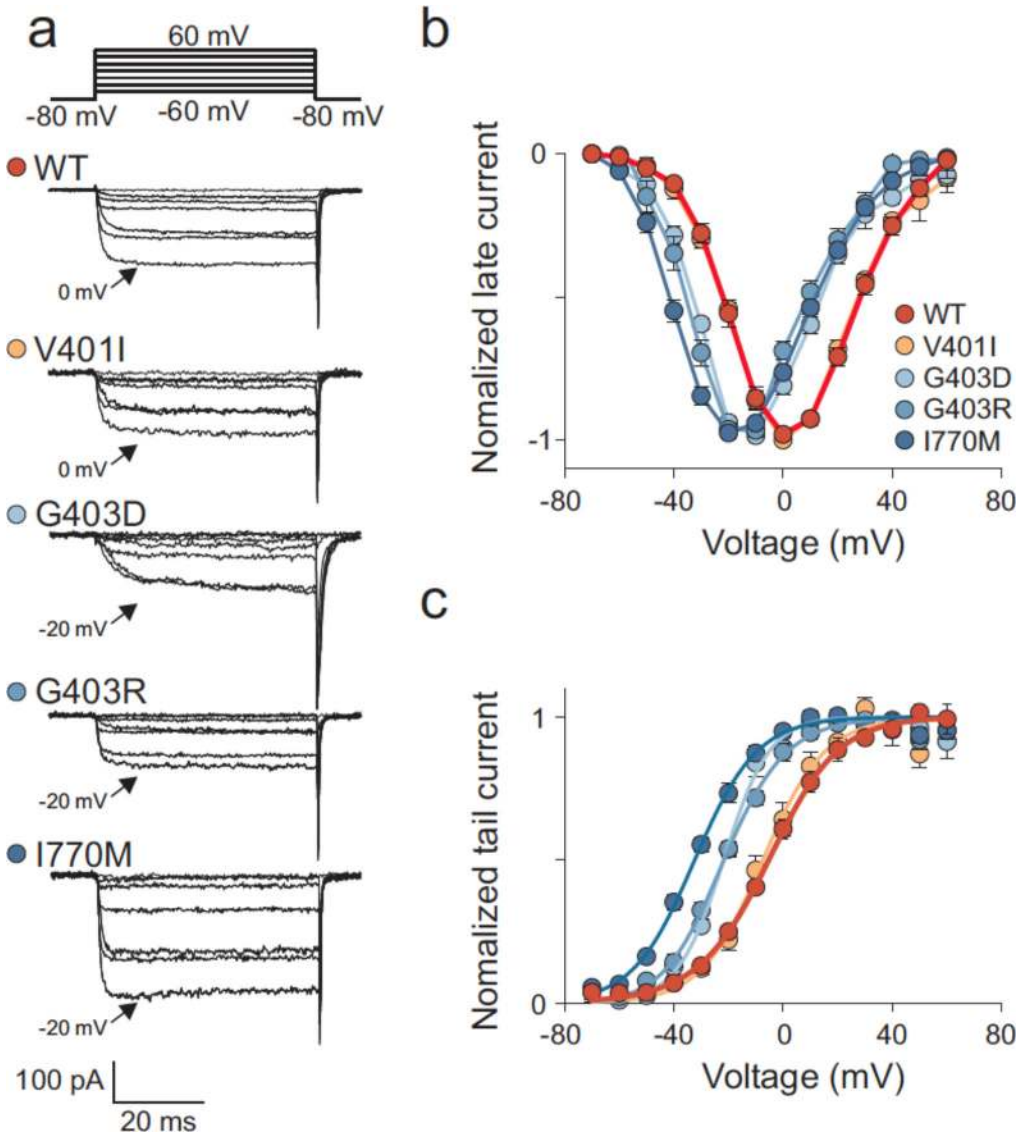

Figure 3.

Immunohistochemistry of $Ca_V1.3$ in human adrenal gland. Human adrenal gland was stained with anti-$Ca_V1.3$ (Sigma) (**a**,**c**) or anti-Dab2 (**b**,**d**, an adrenal glomerulosa marker), and sections were counterstained with haematoxylin. $Ca_V1.3$ is expressed in adrenal glomerulosa. (**a**,**b**), scale bar represents 500 μm; (**c**,**d**), 100 μm. C, capsule; G, glomerulosa; F, fasciculata; R, reticularis.

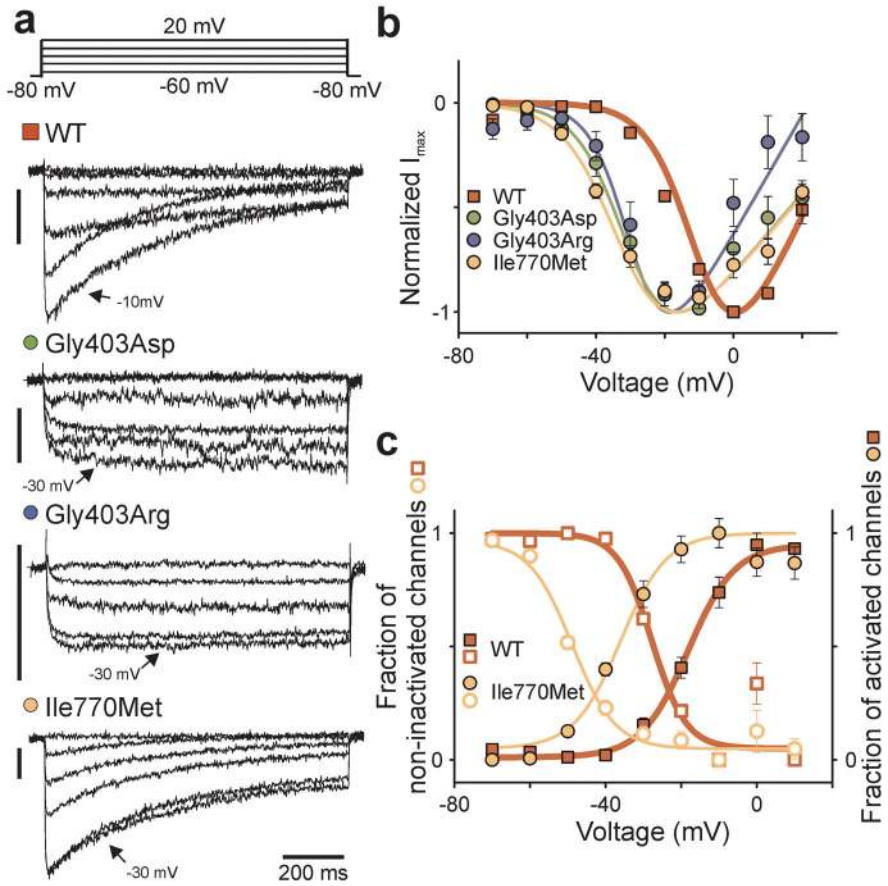

Figure 4.

$Ca_V1.3$ mutations shift the voltage-dependence of activation to more hyperpolarized potentials. (**a**) Representative whole cell recordings of HEK293T cells transiently expressing WT or mutant $Ca_V1.3$ together with β_{2a} and $\alpha_2\delta_1$ subunits (vertical bar: 50 pA). Currents were elicited by voltage pulses between −60 mV and +20 mV including the peak current amplitude (arrow). (**b**) Voltage dependence of normalized peak current amplitudes (I_{max}) of WT (n = 7), Gly403Asp (n = 5), Gly403Arg (n = 7) or Ile770Met (n = 6) channels. The voltage dependence of activation is shifted to more hyperpolarized potentials in Gly403Asp, Gly403Arg and Ile770Met channels. (**c**) Activation (filled symbols) and inactivation (open symbols) curves of WT and Ile770Met channels. Activation and inactivation of Ile770Met channels are both shifted to more hyperpolarized potentials. Activation curves were calculated from **b,** while the inactivation curves were calculated from fits of the inactivation time courses. Data are presented as mean ± s.e.m.